Chemistry and Materials Research
ISSN 2224- 3224 (Print) ISSN 2225- 0956 (Online)
Vol.7 No.1, 2015

Natural Dye Sensitized Solar Cells of Ocium Lamifolium and Tagets Patula Based on Metal Oxide Nanocomposite in Quasi Solid State Electrolyte

Megersa Feyissa Mideksa[1] Abi Tadesse Mengesha[1] Girma Goro Gonfa[2] Teketel Yohannes Ashembo[3]
1.Department of Chemistry, College of Natural and Computational Sciences, Haramaya University, Haramaya, Ethiopia
2.Department of Physics, College of Natural and Computational Sciences, Dire Dawa University, Dire Dawa, Ethiopia
3.Department of Material Science, College of Natural and Computational Sciences, Addis Ababa University, Addis Ababa, Ethiopia
megersafeyissa@yahoo.com;abi92003@yahoo.com;girmag@gmail.com; teketely@yahoo.com

Abstract
Nanocomposite of Sn-Zn oxide from their respective precursor salts was prepared by impregnation method. The prepared nanocomposite was characterized by UV-Vis to estimate optical absorption and energy band gaps and X-ray Diffraction to determine particle size. Absorption spectra of the natural dyes were measured and both ethanol extracts of natural pigments absorbs in the visible region. Morphology of the as-synthesized nanocomposite was characterized by Scanning Electronic Microscopy and Energy-Dispersive X-ray for elemental analysis. The solar energy conversion efficiency of the as-synthesized nanocomposite sensitized by the natural dyes of *Ocium Lamifolium* and *Tagets Patula* extracted by ethanol were measured. The best device parameter was achieved by the ethanol extract of *Tagets Patula* and SnO_2/ZnO nanocomposite semiconductor. The percent incident to photon conversion efficiency of the sensitized nanocomposite was measured at light intensity of 100 mW/cm^2 with highest value 9.30 at 320 nm the highest value percent of fill factor was 65.25 by SnO_2/ZnO semiconductor and *Tagets Patula* dye.
Keywords: semiconductor, impregnation, natural dye, dye sensitized solar cells.

1. Introduction

Among all the renewable energy technologies, such as wind turbines, hydropower, wave and tidal power, solar cells and solar thermal, photovoltaic technology utilizing solar energy is considered as the most promising one. Fortunately, the supply of energy from the sun to the earth is gigantic; 3×10^{24}J a year, or about 10,000 times more than that the global population currently consumes (**Grätzel, 2001**). Nowadays, solar energy is one of the most promising future energy resources in concerns to the sustenance of life on earth and the depletion of fossil fuels. Even before the industrial revolutions human life quality is greatly affected by the availability of energy. The escalated and savage consumption of conventional sources of energy are leading to forecasted energy and environmental crises. Renewable energy sources such as solar energy are considered as a feasible alternative because more energy from sunlight strikes Earth in one hour than all of the energy consumed by humans in an entire year. The solar energy strike to the earth in one hour is about $4.3x10^{20}$ J, which is higher than all the energy consumed in the planet ($4.1x10^{20}$ J). Therefore, covering 0.1% of the earth's surfaces with solar cell of 10% efficiency would satisfy the current energy demand (**Grätzel., 2001**).

Solar cells are one type of photovoltaic cells which use a method of generating electrical power, by converting energy of light into direct current electricity using semiconductors that exhibit the photovoltaic effect. For the photovoltaic effect, electrons are transferred between different bands (usually from the valence bands to conduction bands) within the material resulting in the buildup of voltage between two electrodes. In some photovoltaic cells, the light radiation is sunlight which explains why the devices are known as solar cells (**Brabec *et al.*, 2001**). Among the next generation solar cells, Dye-Sensitized Solar Cells has proven to be a promising new concept, in contrast to conventionally used Si-based solar cells. The main advantages of DSSC are the low-cost manufacturing process (non-purified starting material as compared to Si-cells), the use of metal oxide as a non-toxic supporting material, and the efficient generation of electricity even at disused (neglected) light conditions (**Smestad, 1998**).

The performance of the DSSC is highly dependent on the sensitizer dye and wide band gap material such as TiO_2, SnO_2, ZnO, and Nb_2O_5. TiO_2 is highly preferable due to its ability to resist the continuous transfer of electron under illumination (in the ultraviolet range). When the metal oxide semiconductor film is immersed in the dye, a monolayer of the dye is anchored onto its surface. Excitation of atoms by sun light occurs in the dye and the photogenerated charges are separated at the interface between the dye and metal oxide. Several studies

have addressed the use of SnO_2 and ZnO. Nanostructured metal oxide semiconducting materials are usually used in the fabrication of DSSC due to the large surface area they offer for dye anchoring (**Chen *et al*., 2009**). The charge transport is highly affected by the crystalline quality of metal oxide material; therefore it is important to reduce the charge traps in the films to speed up charge transport. The amount of light entering the DSSCs and the photocurrent extractions are based on the transparent electrode. In the fabrication of DSSCs, the choice of the metal oxide material and the transparent electrode is crucial to obtain efficient light harvesting, charge separation, and extraction. The highest efficiency of DSSCs sensitized by Ru-containing compounds absorbed on nanocrystalline TiO_2 reached 11–12% (**Buscaino *et al*., 2008**). But the new cobalt-based redox couples are the renaissance of dye-sensitized solar cells with higher open-circuit voltages, leading to a new record power-conversion efficiency of 12.3% (**Brian *et al*., 2012**).

Tin oxide (SnO_2) is one of the extensively studied semiconductors for photocatalytic and photoelectrochemical applications. Its potential applications in energy production and storage devices are inevitable. Tin oxide mobility reported in both single crystal SnO_2 (μ ~250 $cm^2V^{-1}s^{-1}$) as well as nanostructures (μ ~125 $cm^2V^{-1}s^{-1}$) are orders of magnitude higher than in both single crystal TiO_2 (μ <1 $cm^2V^{-1}s^{-1}$) and ZnO (μe 1–5 $cm^2V^{-1}s^{-1}$). Furthermore, SnO_2 has a low sensitivity to UV degradation due to its larger band gap and hence has better long term stability. In spite of these advantages the open circuit voltage, V_{oc}, of SnO_2 nanoparticle based DSSCs has been limited to less than 400 mV, making them less attractive (**Senevirathna *et al*., 2007**).

2. Synthesis of oxide nanocomposite

The nanocomposite was performed according to the procedure developed by **Dong et al., (2006)** through impregnation method. 0.1M of binary mixed oxides Sn/Zn were prepared by impregnating $SnCl_4.5H_2O$ with $(CH_3COO)_2Zn.2H_2O$ aqueous solutions. Aqueous solution of ammonia was used for the adjustment of pH. The mixture of solutions were left for four hours for the formation of gel, then dried at 110^oC in an oven over night and further calcined at two steps temperature 350^oC and 550^oC for three hours in each temperature. The synthesized powder was characterized by various instruments to study its various properties.

2.1. Sample Dye collection and preparation

Fresh flowers of *Tagets patula* and *Ocium Lamifolium* plants were collected and dried at room temperature in a shade to prevent dye degradation. After drying for about 2 months the samples were grounded with grinding machine to produce the powder of the respective plant materials.

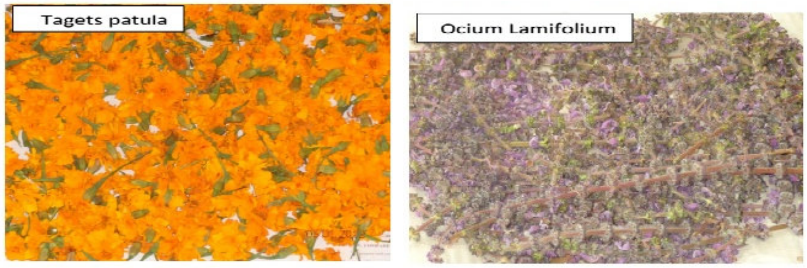

Figure 1. Fresh flower of the collected samples

2.2. Extraction of natural pigments

The extraction of dye was performed as follows: 2 gm of each powder of dyes sample were taken and soaked in 50 mL of ethanol for extracting using ethanol. The same amount of powder was soaked in 50 mL of water for water extracting and 50 mL of 0.1M HCl for HCl extracting in separate bottle. The solution was kept at room temperature for about 12 hours to extract the dye completely. Then the solution was filtered with glass filter to separate the solid from the pure liquid.

2.3. UV-Visible absorption measurement

From each as-synthesized nanocomposite, small amount of the sample was taken and dissolved in ethanol. The absorption edge of all samples were measured by scanning from 200 - 500 nm and for the extracted natural dyes absorption edge were measured by scanning from 200 - 800 nm by using UV-visible spectrophotometry.

2.4. XRD analysis

To characterize crystal structure and phase of the powder nanocomposite, small amount of the powders were taken and ground to fine particle and analyzed by XRD equipped with a Cu target for generating a Cu Kα radiation with λ = 0.15406 nm. The 2θ record ranging from 4^0–64^0 while the accelerating voltage and applied current was held at 40 kV and 50 mA, respectively. The particle size (D) of the powders was calculated by

Scherer's Formula;

$D = K\lambda / \beta Cos\theta = 0.90\lambda/\beta Cos\theta$ (1)

Where,

K= 0.90 is the Scherer's constant, λ is the x-ray wave length, θ is the Bragg's diffraction angle, 2θ is the angle between the incident and diffracted x-ray, and β is the peak width of the diffraction line at half of the maximum intensity.

2.5. Scanning electron microscopy (SEM)

Morphologies and thickness of the samples were investigated by scanning electron microscope (SEM) instrument operating at constant beam energy. To prepare the sample small amount of the as-synthesized nanocomposite was taken and placed in the pellet maker. The powder was then compressed with a high pressure. The SEM images were captured at different magnification levels and the morphological features of the particles were studied.

2.6. Energy dispersive X-ray (EDX)

The elemental analysis or chemical composition of the as-synthesized nanocomposite was done by using energy dispersive x-ray at the electron microscope unit (EMU). To prepare the sample small amount of the as-synthesized nanocomposite was scooped and placed in the pellet maker. The prepared pellet was then coated with carbon before mounting in the machine. The powder was then compressed with a high pressure. The operation was done at excitation energy of 20 keV with scan or acquisition time of 600s.

2.7. Paste Preparation

0.8ml of a dispersing agent, PEG, 1 ml of ethanol and 4 drops of triton were mixed. 3 gm of as-synthesized nanocomposite was continuously grounded by using porcelain mortar and pestle to break down the aggregated particle. Then 1 mL of the mixture of acetonitril, triton and PEG solution was slowly added to the powder and completely mixed by using the mortar and pestle. Finally the paste was ready for deposition. The film was prepared through **Doctor Blade** method and sintered 430^{o}C for 30' to evaporate the solvent used and to bind the paste with the ITO glass.

2.8. Preparation of quasi solid state electrolyte

The polymer gel electrolyte was prepared according to the method developed by **Kang et al. (2010)** as described below;

0.9 M of 1-ethylene-3-methyl imidazolium iodide was added into acetonitrile under stirring to form a homogeneous liquid electrolyte. In order to obtain a better conductivity, 0.5 M of sodium iodide was dissolved in the above homogeneous liquid electrolyte and then 0.12 M iodine and 35% (w/w) of PVP were added. Then, the resulting mixture was heated at 70 - 80^{o}C under vigorous stirring to dissolve the PVP polymer, followed by cooling down to room temperature to form a gel electrolyte and stored in discator.

2.9 Coating counter electrodes

A three-electrode electrochemical cell was used for polymerization of EDOT. The poly(3,4-ethylenedioxythiophene) (PEDOT) film for the counter electrode was formed by electrochemical polymerization of 3, 4-ethylenedioxythiophene (EDOT) in a three electrode one-compartment electrochemical cell. The electrochemical cell consisted of a pre-cleaned ITO-coated glass working electrode, platinum foil counter electrode and quasi Ag/AgCl reference electrode were dipped in $(C_2H_5)_4NBF_4$ acetonitrile solution. The solution used for polymerization contained 0.1 M EDOT and 0.1 M $(C_2H_5)_4NBF_4$ in acetonitrile. The monomer was used as received. The polymerization was carried out potentiostatically at +1.8 V for 20 seconds. At this potential, the electrode surface becomes covered with blue-doped PEDOT film. Then the film was rinsed with acetonitrile and dried in air.

2.10. Assembly of DSSCs for characterization

Device assembly is the final step for characteristics measurement. The sensitized electrode was washed by the solvent of the dye followed by ethanol and dried using hair dryer to dry the electrode and then the uncovered part of the film by the paste was covered by a tape spacer in all side by leaving some place for electrical contact. By facing up the active sides of the photoanode and the cathode, the two electrodes were pressed together after putting the quasi solid electrolyte on the photoanode. Then the devices were ready for characterization.

3. RESULT AND DISCUSSION

3.1. UV-visible absorption measurement of dyes

The UV–vis absorption spectra of ethanol, HCl and water extracts of *Ocium Lamifolium* and *Tagets Patula* were

investigated. Figure 2 show the UV–Vis absorption spectra of dyes extracted by ethyl alcohol, water and hydrochloric acid. From the two figures, the *Ocium Lamifolium* extract of ethanol shows more than one peak and for which shows only one peaks, and the hydrochloric acid extract of *Tagets Patula* dyes shows three absorption peaks in the visible region and no peak observed for water extract of both dyes. This indicate that the dye present in the *Tagets Patula* has acidic property compaired to that of *Ocium Lamifolium* dye which shows only one peak with acid extarcts.

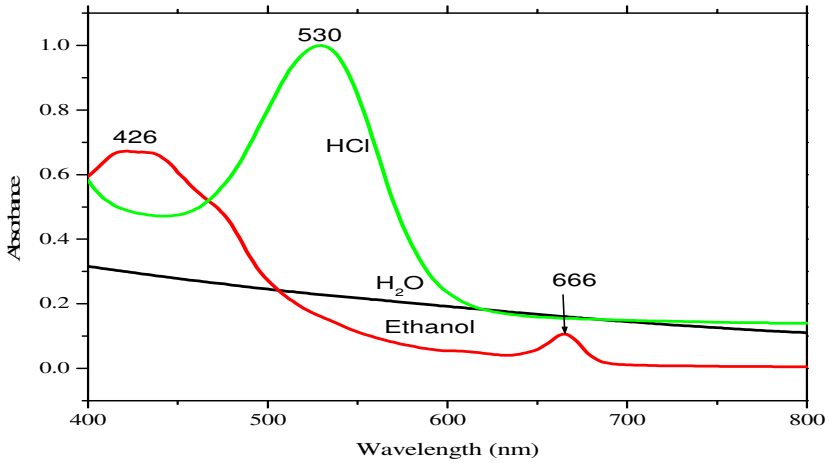

Figure 2. Absorption spectra of *Ocium Lamifolium* by water. HCl and Ethanol

For ethanol extract the maximum absorption peak around 420 nm with a corresponding peak around 663 nm which are indicative of the presence of chlorophyll a. The peaks at 530 nm for 0.1 M HCl is indicative of the presence of anthocyanins which may be responsible for its coppery appearance **(Godibo, 2012)**. No absorption measured for water extract above 400nm which indicates that the dyes extract by water are not absorbed in visible region spectrum.

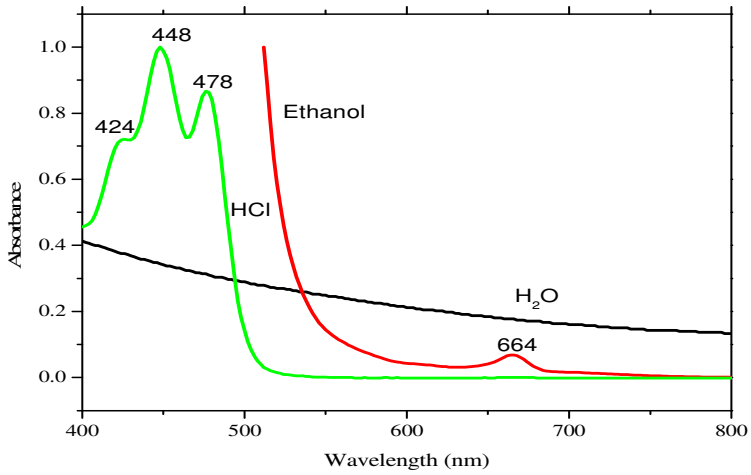

Figure 3. Absorption spectra of *Tagets Patula* by water, ethanol and HCl

For ethanol extract of *Tagets Patula* the maximum absorption peak around 664 nm is indicative of the presence of chlorophyll a. The three peaks at 424, 448 and 478 nm for 0.1 M HCl are indicative of the presence of anthocyanins.

The natural dyes extracted from the various plants have complicate mixed constituents, which causes no single absorption wave of light. Thus, in all cases of water extract a dye doesn't show any absorption peak, this does not mean that there is no pigment that extract by polar solvent. Instead it is due to the existance of anthocyanin in two form, in flavylium cation and quinonoidal form. When this sample is acidified an absorption band which is a characteristic of anthocyanins starts to be observed due to the shift in equilibrium from quinonoidal to flavylium form. In this pigment, the aqueous environment available in large quantity was add to the flavyllium form at pH values above 1.5 - 2.0, resulting in a loss of color owing to the formation of the colorless pigment through a slow acid-base equilibrium. But in general the dyes used in these studies are effective photo-receptors because they contain networks of alternating single and double bond.

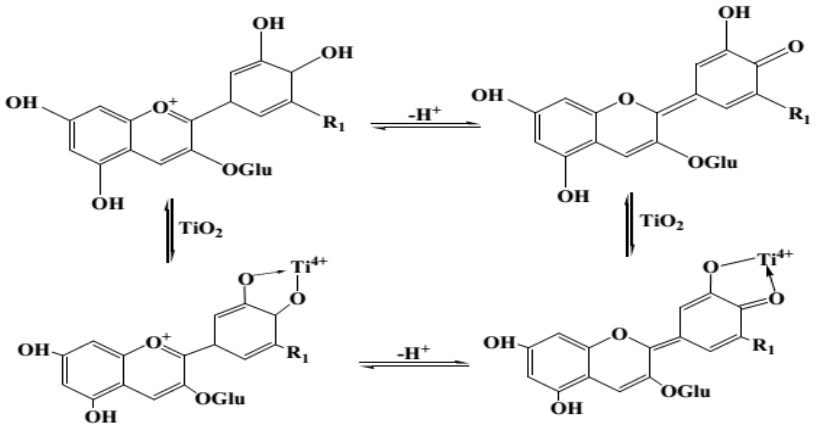

Figure 4. Equilibrum between Flavyllium and Quinonoidal **(Sisay *et al*., 2012)**

3.2. UV-Visible spectra of as-synthesized nanocomposite

An aqueous suspension of the sample was used for the UV-Vis absorption studies. The absorption spectrum of as-synthesized nanocomposite was measured by UV-visible spectroscopy. The band edge of each nanocomposite was determined from its absorption age with respect to the wavelength or from direct re-plotted spectra of $(\alpha h\nu)^{1/2}$ vs hν (commonly known as Tauc plot) by considering SnO_2 to be direct transition semiconductor and ZnO to be an indirect semiconductor where α adsorption coefficient and ν light frequency **(yunfang *et al*., 2013)**.

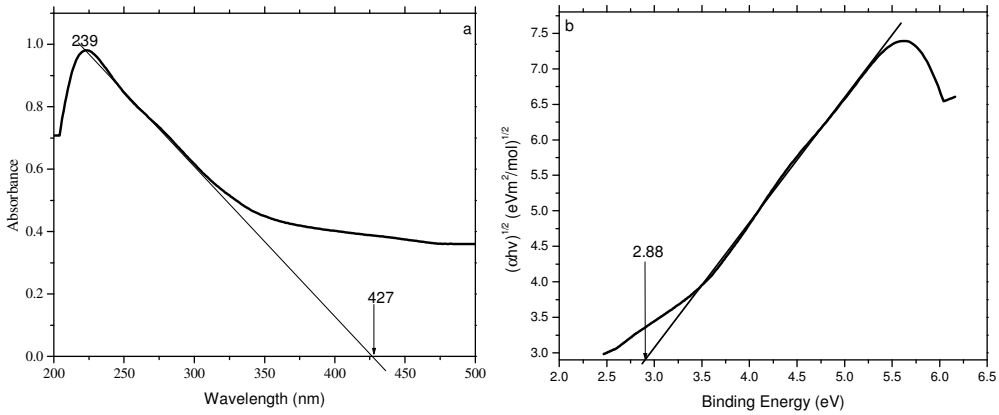

Figure 5. Optical Absorption (a) and band gaps (b) of mixture of Tin and Zinc oxides

From the figure described above, the band age of the as-synthesized nanocomposite was determined either from the direct re-plotted spectrum or by calculating form absorption edges using the Scherer's Formula. The obtained band ages is less than the band age of both tin oxide and zinc oxide normally what they had, because when zinc oxide couples with SnO_2 semiconductor, the conduction band of SnO_2 acts as a sink for photogenerated electrons. The photogenerated holes move in the opposite direction, accumulate in the valence band of ZnO particles, which leads to an increase in charge separation efficiency and extends the photo responding range to visible light.

3.3 XRD Analysis

As a primary characterization tool for obtaining critical features such as crystal structure, crystallite size, and strain, x-ray diffraction patterns have been widely used in nanoparticle research. For these study the Bruker D8 X-ray diffractometer (XRD) operating with monochromatic high intensity Cu Kα (λ= 0.15406 nm) radiation was used. The x-ray diffraction pattern of the as-synthesized nanocomposite of SnO_2/ZnO sample was shown in Figure 6. The results show distinct peaks with their corresponding 2θ and β values (given in units degree and radians, respectively) which accounts for the crystalline nature of all the as-synthesized powders. Using equation (1), the average crystallite sizes of the as synthesized semiconductors were calculated and given in Table 1.

Table 1. Crystal size and energy bandgap of the as-synthesized nanocomposite

Nanocomposite	2θ (degree)	β (radians)	D (nm)	Bandgap (E_g) (eV)
SnO_2/ZnO	26.898	0.0133	10.72	2.88

The smaller particle size for the mixed oxide could be attributed to an increase in the surface area and the resistance to sintering caused by the doped oxide. As shown in Table 1, the as-synthesized powders are in nanorange.

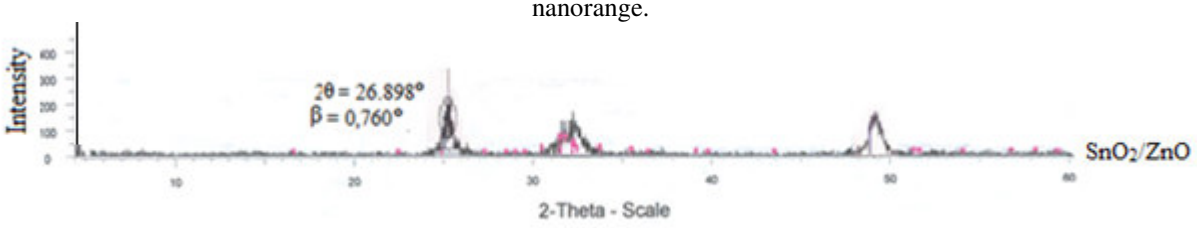

Figure 6. XRD pattern of the as-synthesized nanocomposite.

3.4 SEM analysis

Field emission gun scanning electron microscopy (SEM) was used to investigate surface topography and particle morphology of the materials. The SEM images of selected as-synthesized nanocomposite with selected magnification are shown in Figure 7. The binary SnO_2/ZnO composite SEM image exhibits white snow flake-like hillocks of SnO_2 particles, mostly aggregated and hexagonal shape of ZnO. The mean particle size of the as-synthesized nanopowder from the SEM image was in μm which is greater compaired to XRD determined particle size. An increment in particle size of printed thick film form of as-synthesized nanopowder was due to the firing at high temperature, resulting particle binding agglomeration similar work with **Ansari et al. (2002)**.

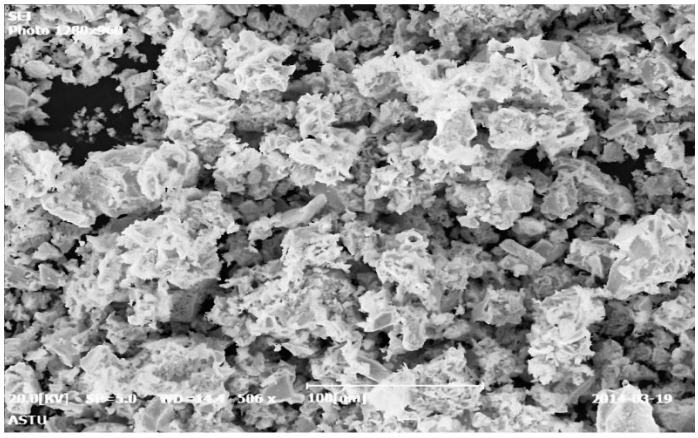

Figure 7. Scanning Electronic Microscopic images of SnO_2/ZnO

3.5 EDX analysis

The energy disperses X-ray spectroscopic analysis was for elemental composition present in the as-synthesized nanopowders, performed coupled to a scanning electron microscope.

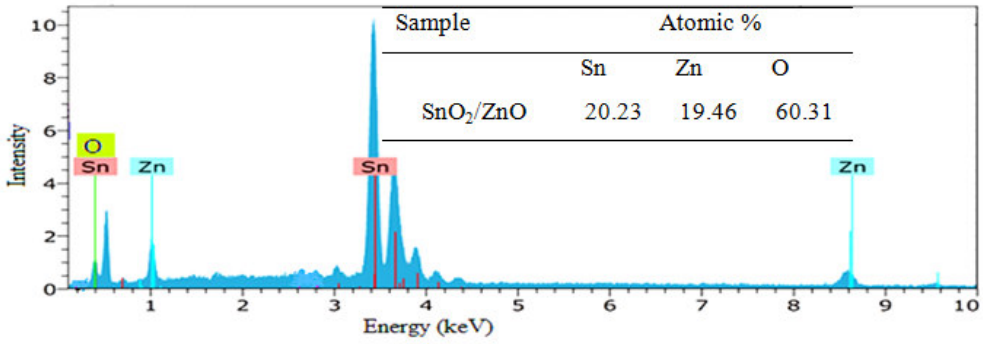

Figure 8. EDX spectrum of SnO_2/ZnO

From the percentage of the as-synthesized nanocomposite given, the atomic percent of oxygen present is relatively triplicate of tin and zinc and the percent of tin and zinc are almost the same confirming the as-synthesized powder chemical composition to be SnO_2/ZnO.

3.6 J-V characterization

The J-V characterization of the as-synthesized nanocomposite and natural dyes with current density versus potential measurement was done. The result obtained for the as-synthesized nanocomposite and ethanol extracted natural dyes shown in Figure 12. The solar cells application was performed for the prepared thin films only by ethanol because the tin containing film was soluble in HCl and the water extract of dyes doesn't show peaks in visible ranges.

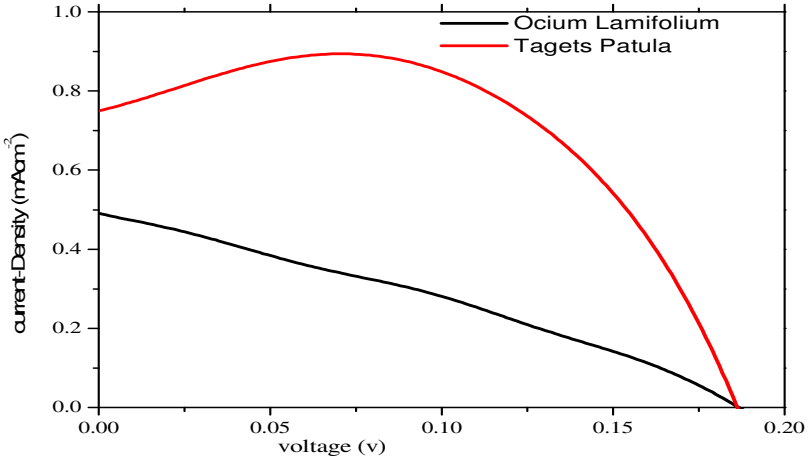

Figure 9. J-V characteristic of the as-sensitized nanocomposite and natural dyes of *Ocium Lamifolium* and *Tagets patula* dyes.

From the J-V characteristic curve of the as-synthesized nanocomposite and the natural dyes, the highest efficiency were obtained with the composition of SnO_2/ZnO and *Tagets Patula*. The reason for the differences may due to the electron transport differences of the as-synthesized nanocomposite and also low temperature calcination at 350 and 550^oC causes significant increasing of electron transport because of lower enegy band between VB and CB which decreases the electron recombination. SnO_2 is supposed to mediate the transport of photogenerated electrons to the electrode substrate through the SnO_2/ZnO film by reducing both the recombination of e^-- h^+ and the back reaction of e^- and the adsorbed oxygen. In addition, from the SEM analysis the SnO_2/ZnO contained electrodes show white snow flake-like hillocks of SnO_2 particles, mostly aggregated and hexagonal shape of ZnO, which can be expected to possess higher surface area for interfacial charge transfer and absorption of the incident illumination, leading to an enhancement in photocurrent. The performance of the DSSCs based on as-synthesized nanopowder in terms of short-circuit photo-current (J_{sc}), open-circuit voltage (V_{oc}), fill factor (FF), and energy conversion efficiency (η) of *Tagetes Patula* and *Ocium lamifolium* which were extracted using the same solvent ethanol were constracted and are shown in Table 3.

Tabel 1. Photovoltaic performance of metal oxides based on DSSCs with natural dyes sensitizers

Sensitizer	Semiconductor	J_{sc} (mA.cm^{-2})	V_{oc} (V)	FF %	η%	IPCE %
Tagets Patula	SnO_2/ZnO	0.125	0.737	65.25	0.092	7.58
Ocium lamifolium	SnO_2/ZnO	0.102	0.276	30.77	0. 028	9.30

Natural dye sensitizers achieve the highest efficiency with the SnO_2/ZnO semiconductor and *Tagets Patula* sensitizer due to the low energy between conduction band and valance band of the semiconductor resulting with faster electron transport and stability of the nanocomposite and the dye extract by ethanol from *Tagets Patula* shows only one peak which responsible for single complex presence, absorbing light of selected wavelength. But in case of the ethanol extract of *Ocium Lamifolium* there are two peaks which can responsible to absorve light with different wavelength. Since the efficient light conversion is measured at specific wavelength, the dye with more than one absorption peak must be further separated in order to obtain specific wave length with efficient light conversion. The CB and VB of semiconductor can be calculated according to the empirical equation developed by **Wang et al. (2012)** and **Cao et al. (2012)**:

$$E_{CB} = \chi\text{-}E_e\text{-}0.5E_g \quad (2)$$

Where E_{CB} is the conduction band edge potential, E_e is the energy free electrons on the hydrogen scale (about 4.5

eV), E_g is the band gap energy of the semiconductor, χ is the electronegativity of the semiconductor, which is the geometric mean of the electronegativity of the constituent atoms and determined for the semiconductor by Sanderson's principle. The E_{VB} can be determined by $E_{VB} = E_{CB} + E_g$. The highest efficiency obtained by the natural dye sensitizer extracted by ethanol was 0.092% with Short-circuit current (J_{sc}) 0.125mAcm^{-2} and open circuit voltage (V_{oc}) 737 mV with *Tagets Patula* and SnO_2/ZnO semiconductor. This comparison is to show the stability of tin oxides with zinc oxide rather than other metal oxides to resist electron injection during long sealing of the nanocomposite in DSSCs.

3.7. IPCE percentage characterization

The incident photon-to-photocurrent conversion efficiency (IPCE) was determined by measuring the photocurrent of as-synthesized nanopowder and natural dyes electrode at different excitation wavelengths. IPCE, defined as the number of electrons generated by light in the external circuit divided by the number of incident photons at each wavelength. The IPCE can be calculated according to equation **(Halme *et al.*, 2010)**.

$$\text{IPCE}\ (\%) = \left(\frac{1240\ \text{Jsc}}{\lambda\ \text{Pin}}\right) \text{x}\ 100 \qquad (3)$$

Jsc is the short circuit current density, λ is the wavelength of the incident light and Pin is the intensity of the incident light. Photo action spectra provided further insights on the photoelectrochemical behavior of natural dyes.

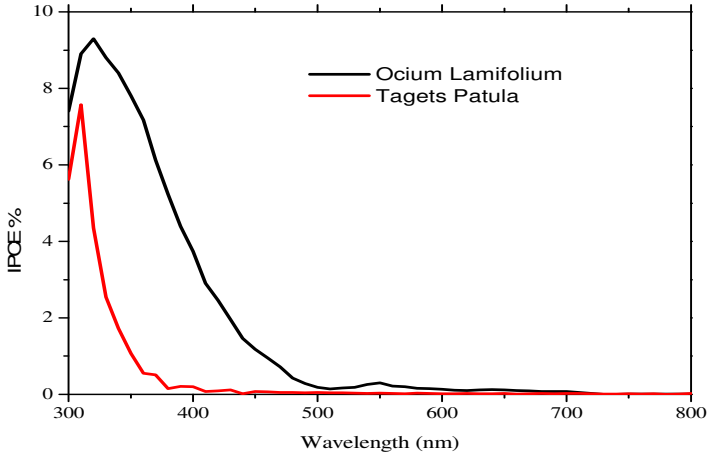

Figure 10. IPCE % characteristics of ethanol extract *ocium Lamifolium* and *Tagets Patula* based on SnO_2/ZnO semiconductor

The conversion efficiency of as-synthesized nanocomposite based on DSSCs improves by reducing the recombination with core shell structure of SnO_2 relatively wider band gap metal oxide (**Senevirathna *et al.*, 2007; Kar and Patra 2009**). As shown from Figure 13, the highest photon to incident conversion efficiency of the as-synthesized nanocomposite is higher than that of natural dyes used. This is because of the small absorption of dyes by the sensitized nanocomposite and from the three sensitized nanocomposite the binary SnO_2/ZnO shows absorption in visible range of wave length. Even though the ZnO nanoparticle is not stable upon mixing with stable SnO_2 gives better stability and large absorption of dye molecule which also reported by **Tennakone et al. (1999)**. The photon to incident conversion efficiency depends on the light absorption efficiency of dyes, electron injection efficiency from LUMO of dye to conduction band of metal oxides and electron collection efficiency of metal oxides. The charge separation depends, on the driving force for electron injection from the LUMO of the dye to the conduction band of the semiconductor oxide, but also, as recently reported (**Cai *et al.*, 2011**), on the populations of the acceptor and donor levels in the injection process and the corresponding back process (electron dye-recombination). The electron collection efficiency is an indication of the probability that a photogenerated electron reaches the collecting substrate contact before it is lost by recombination **(Halme *et al.*, 2010)**. The collection efficiency thus depends on the average distance that electrons travel before recombination. **Figure 10**. elaborate such parameters easily.

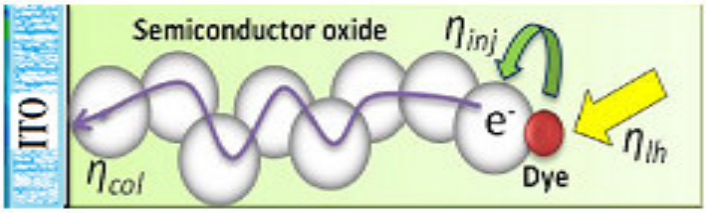

Figure 11. Scheme of the processes IPCE of DSSCs **(Halme *et al*., 2010)**

Conclusion

A semiconductor of SnO_2/ZnO nanocomposite were synthesized by using impregnation method and characterized to provide energy barrier at the electrode/electrolyte interface which gives a reduced recombination of photoinduced electrons and characterized to study its various properties. For the as-synthesized nanocomposite and natural dyes, the optical absorption was measured resulting UV range for the nanocomposite and visible range for the natural dyes extracted by ethanol and hydrochloric acid indicating both are photoactive dyes. From XRD result, the as-synthesized powder was nanosized semiconductors. In order to investigate the elemental component and the morphology of the as-synthesized nanopowder, the energy dispersive x-ray (EDX) and scanning electronic microscopy (SEM) respectively, were performed resulting only the expected element are present in the nanocomposite with irregular shape. DSSCs were fabricated using SnO_2/ZnO nanocomposite for both natural dyes sensitizers and their photovoltaic performance were determined.

Reference

Ansari, Z. A., S. G. Ansari, T. Ko and J. H. oh, 2002. Effect of MoO_3 doping and grain size on SnO_2-enhancement of sensitivity and selectivity for CO and H_2 gas sensing. *Sens. Actuator B*, 87: 105-114.

Brabec, C., N. Sariciftci and J. Hummelen, 2001. Plastic solar cells. *Adv. Funct. Mater.,* 11(1): 15–26.

Brian, E. H., H. J. snaith and M. D. McGehee, 2012.The renaissance of dye-sensitized solar cells. *Nat. Photon*., 6: 4038-4045.

Buscaino, R., C. Baiocchi, C. Barolo, C. Medana, M. Gratzel, Md.K. Nazeeruddin and G. Viscardi, 2008. A mass spectrometric analysis of sensitizer solution used for dye sensitized solar cell. *Inorgan. Chem.*, 361: 798–805.

Cai, J., N. Satoh and L. Han, 2011. Injection Efficiency in Dye-Sensitized Solar Cells within a Two-Band Mode. *J. Phys. Chem*., 115: 33-60.

Cao, J., B. D. Luo, H. L. Lin, B. Xu, S. Chen and J. Hazard, 2012. Enhanced photocatalytic activity of Ag/Ag_3PO_4 coaxial hetero-nanowires. *Mater.* 217-218: 107-115.

Chen, H., Z. Duan, Y.G. Lu and A. D. Pasquier, 2009. Dyesensitized solar cells combining ZnO nanotip arrays and nonliquid gel electrolytes. *J. electron mater.*, 38:1612-1617.

Dong, X., H. Zou and W.Lin, 2006. Effect of preparation condition of CuO-CeO2-ZrO2 catalyst on CO removal from hydrogen rich gas, *int. J.hydr. energ.*, 31: 234-237.

Godibo, D. J., 2012. Screening of Natural Dyes for Use in Dye Sensitized Solar Cells. *A. A. Ethio*., 70.

Gratzel, M. 2001. Molecular photovoltaics that mimic photosynthesis. *Pure Appl. Chem.*, 73(3): 459–467.

Halme, J., P. Vahermaa, K. Miettunen and P. Lund, 2010. Natural dye sensitized phothoelectrochemical cells based on zinc oxide nanoparticles. *Adva. Mate*., 22: 210-221.

Kara**,** A**.** and Patra A**.,** 2009**.** Optical and electrical properties of Eu^{3+}-doped SnO_2 nanocrystals. *J. Phys. Chem. C*, 113: 4375–4380.

Kang, S. , J. Wu, S. Hao, Z. Lan and J. Lin, 2010. Natural dye sensitized phothoelectrochemical cells based on zinc oxide nanoparticles. *Ener. Sour*., 32:15-68.

Senevirathna, M. K. I., P. K. D. D. P. Pitigala, E.V. A. Premalal, K. Tennakone, G. R. A. Kumara and A. Konno, 2007. Stability of the SnO_2/MgO dye-sensitized photoelectrochemical solar cell. *Sol. Energ. Mater. Sol. Cells*, 91: 544–547.

Smestad, G. P., 1998. Education and solar conversion. *Sol. Energ. Mater.*, 55(1-2): 157-178.

Sisay, T., A. Atakilt, C. Yonas, G. I. Villar, Y. Teketel, 2012. Natural dye-sensitized solar cells using pigments extracted from Syzygium guineense. *J. Photon. Ener.*, 2(1): 1-10.

Tennakone, K., G. R. R. Kumara, I. R. M. Kottegoda and V. P. S. Perera, 1999. Dye-sensitized photoelectrochemical cells based on porous SnO_2/ZnO composite and TiO_2 films with a polymer electrolyte. *Chem. Commun*., 11: 2474 - 2477.

Wang, H., J. Gao, T. Q. Guo, R. M. wang, L. Guo, Y. Liu, J. H. Li, 2012. Advanced nanoarchitectures of silver/silver compound composites for photochemical reactions. *Chem.commun.*, 48: 275-277.

Yunfang, W., L. Xiuli, W. Yawen and F. Caimei, 2013. Novel visible-light AgBr/Ag_3PO_4 hybrids photocatalysts with surface plasma resonance effects. *J. Solid State Chem*., 202: 51-56.

The IISTE is a pioneer in the Open-Access hosting service and academic event management. The aim of the firm is Accelerating Global Knowledge Sharing.

More information about the firm can be found on the homepage:
http://www.iiste.org

CALL FOR JOURNAL PAPERS

There are more than 30 peer-reviewed academic journals hosted under the hosting platform.

Prospective authors of journals can find the submission instruction on the following page: http://www.iiste.org/journals/ All the journals articles are available online to the readers all over the world without financial, legal, or technical barriers other than those inseparable from gaining access to the internet itself. Paper version of the journals is also available upon request of readers and authors.

MORE RESOURCES

Book publication information: http://www.iiste.org/book/

Academic conference: http://www.iiste.org/conference/upcoming-conferences-call-for-paper/

IISTE Knowledge Sharing Partners

EBSCO, Index Copernicus, Ulrich's Periodicals Directory, JournalTOCS, PKP Open Archives Harvester, Bielefeld Academic Search Engine, Elektronische Zeitschriftenbibliothek EZB, Open J-Gate, OCLC WorldCat, Universe Digtial Library , NewJour, Google Scholar